THE ASTROPHYSICAL JOURNAL SUPPLEMENT SERIES, 138:63–74, 2002 January

ARECIBO OBSERVATIONS OF FORMALDEHYDE AND RADIO RECOMBINATION LINES TOWARD ULTRACOMPACT H II REGIONS

ESTEBAN ARAYA
University of Puerto Rico at Río Piedras, Physics Department, P.O. Box 23343, San Juan, PR 00931
PETER HOFNER
University of Puerto Rico at Río Piedras, Physics Department, P.O. Box 23343, San Juan, PR 00931; and Arecibo Observatory, NAIC/Cornell University
ED CHURCHWELL
University of Wisconsin-Madison, Astronomy Department, 475 North Charter Street, Madison, WI 53706
AND
STAN KURTZ
Instituto de Astronomía, UNAM, Apartado Postal 70-264, México, DF, 04510, Mexico
Received 2001 June 27; accepted 2001 August 27

ABSTRACT

We report observations of the H110α radio recombination line and H_2CO (1_{10}–1_{11}) toward 21 ultracompact H II regions with the Arecibo 305 m radio telescope. We detect the H110α line in 20 sources, and for each of these we also detect a H_2CO absorption feature at nearly the same velocity, demonstrating the association between molecular and ionized gas. We determine kinematic distances and resolve the distance ambiguity for all observed H II regions, as well as for 19 intervening molecular clouds. A plot of the Galactic distribution of these objects traces part of the spiral structure in the first Galactic quadrant. We compare flux densities and velocities as measured with the Arecibo Telescope with interferometric measurements of our sample of ultracompact H II regions. In general, the single-dish fluxes exceed the interferometric values, consistent with an extended component of radio continuum emission.

Subject headings: Galaxy: structure — H II regions — ISM: molecules — radio lines: ISM

1. INTRODUCTION

One of the earliest observable manifestation of massive star formation are ultracompact H II (UCH II) regions. Interferometric measurements of the free-free emission from the ionized gas have resulted in a large number of images of these regions at arcsecond and subarcsecond resolution (e.g., Kurtz, Churchwell, & Wood 1994). The small size of UCH II regions, together with the high thermal pressure of the ionized gas, suggests that these objects are quite short-lived and should rapidly expand out of the ultracompact phase. This is in contradiction with the large number of UCH II regions observed and is commonly referred to as the "Life Time Problem" (Wood & Churchwell 1989). Among the many theoretical models proposed to explain this problem (see Churchwell 1999 and Kurtz et al. 2000 for a summary), it was recently pointed out by Kurtz et al. (1999) and Kim & Koo (2001) that many UCH II regions are embedded in regions of extended radio continuum emission, which if ionized by the same stars, may imply much greater ages for the ionizing stars, and higher luminosities. The extended radio continuum emission is not detected in interferometric measurements due to missing short *uv*-spacings and can only be fully detected using single-dish measurements. We have used the Arecibo 305 m radio telescope[1] to simultaneously measure the 6 cm radio continuum and the H110α radio recombination line (RRL). The RRL measured with the single-dish Arecibo beam of FWHM 1′ is likely dominated by the extended component of ionized gas and therefore allows a comparison of the ionized gas velocity between ultracompact and extended components.

[1] Arecibo Observatory is part of the National Astronomy and Ionosphere Center (NAIC) which is operated by Cornell University under contract with the National Science Foundation.

The new correlator of the Arecibo Telescope permitted simultaneous observations of the H110α line and the $J_{KaKc} = 1_{10}$–1_{11} transition of interstellar formaldehyde (H_2CO) in absorption against the 6 cm radio continuum. This provides an ideal method for deriving kinematic distances and resolving the distance ambiguity for our sample of UCH II regions. Many of our targets have previously determined kinematic distances based on single-dish observations of hydrogen radio recombination lines (Lockman 1989) and H I absorption line experiments, (Kuchar & Bania 1994). Compared with these earlier distance determinations, our data have the advantage that they were taken with a HPBW 3 times smaller and are thus better matched to the size of compact and ultracompact H II regions. Furthermore, because the 1_{10}–1_{11} transition of interstellar H_2CO generally occurs only in absorption, the interpretation of our data is more straightforward than the single-dish H I data. The H_2CO data also permit us to determine the locations of the intervening molecular clouds.

Section 2 describes our observations and data reduction. In § 3 we discuss our main results, and our conclusions are summarized in § 4.

2. OBSERVATIONS AND DATA REDUCTION

We performed observations toward 21 UCH II regions with 6 cm flux densities larger than 0.08 Jy selected from previous interferometric observations by Afflerbach et al. (1996), Kurtz et al. (1994), and Wood & Churchwell (1989). The data were collected between 2000 September 15–18 with the 305 m Arecibo Telescope. We observed the H_2CO (1_{10}–1_{11}) transition ($\nu_0 = 4829.6594$ MHz for $F = 2$–2), as well as H110α ($\nu_0 = 4874.1570$ MHz) toward the 21 UCH II regions listed in Table 1 using the new C-band Gregorian system. The beamwidth of the Arecibo Telescope at 4.85

TABLE 1

OBSERVED SOURCES

Source	α(1950)	δ(1950)	References S[a] V[b] D[c]
G32.80+0.19.....	18 47 57.0	−00 05 34	1 1 1
G33.13−0.09.....	18 49 34.3	+00 04 31	1 1 1
G33.92+0.11.....	18 50 17.5	+00 51 46	3 - 4
G34.26+0.15[d].....	18 50 46.1	+01 11 13	3 1 4
G35.20−1.74[e].....	18 59 14.0	+01 09 02	3 3 3
G35.57−0.03.....	18 53 51.4	+02 16 28	2 - 5
G35.58+0.07.....	18 53 31.1	+02 19 15	2 - 5
G37.87−0.40.....	18 59 24.5	+04 08 27	2 1 1
G41.74+0.10.....	19 04 50.5	+07 47 59	3 - -
G43.89−0.78.....	19 12 02.8	+09 17 19	3 - 4
G45.07+0.13.....	19 11 00.4	+10 45 43	3 6 8
G45.12+0.13.....	19 11 06.2	+10 48 26	3 1 1
G45.45+0.06.....	19 12 00.1	+11 04 00	3 1 1
G45.47+0.05.....	19 12 04.3	+11 04 11	3 - 8
G48.61+0.02[f].....	19 18 12.9	+13 49 43	2 - 2
G50.32+0.68.....	19 19 11.4	+15 38 37	3 - 8
G60.88−0.13[g].....	19 44 13.5	+24 28 00	2 - 2
G61.48+0.09[h].....	19 44 43.5	+25 05 22	3 - 3
G69.54−0.98[i].....	20 08 09.9	+31 22 39	2 - 9
G70.29+1.60[j].....	19 59 50.0	+33 24 20	7 7 1
G70.33+1.59[k].....	19 59 58.5	+33 25 50	7 7 1

NOTE.—Units of right ascension are hours, minutes, and seconds, and units of declination are degrees, arcminutes, and arcseconds.

[a] Reference for the UCH II region flux density.

[b] Reference for the UCH II region velocity.

[c] Reference for previously determined distance.

[d] W44.

[e] W48.

[f] W51D.

[g] S87.

[h] S88B.

[i] ON 1.

[j] K3–50A.

[k] K3–50C.

REFERENCES.—(1) Afflerbach et al. 1996; (2) Kurtz et al. 1994; (3) Wood & Churchwell 1989; (4) Kuchar & Bania 1994; (5) Downes et al. 1980; (6) Lim & White 1999; (7) Roelfsema et al. 1988; (8) Churchwell et al. 1990; (9) MacLeod et al. 1998.

GHz is approximately 1′. We observed both spectral lines simultaneously using four independent boards of the correlator to process both linear polarizations. We used 2048 channels per subcorrelator, nine-level sampling and a channel width of 3.05 kHz (0.188 km s^{-1}). The total bandwidth of 6.25 MHz resulted in a usable velocity coverage of about 400 km s^{-1}. The central radial velocity in each board was at $V_{LSR} = 0$ km s^{-1} for the relevant spectral line.

TABLE 2

CALIBRATORS

Source	α(1950)[a]	δ(1950)[a]	Flux Density[b] (Jy)
B1843+0950.....	18 43 15.3	+09 50 31.3	1.78
B1857+1255.....	18 57 04.5	+12 55 00.9	0.91
B2001+1357.....	20 01 00.5	+13 57 25.3	0.45
B2018+2932.....	20 18 03.9	+29 32 43.5	4.06

[a] Positions from NVSS Survey (Condon et al. 1998). Units of right ascension are hours, minutes, and seconds, and units of declination are degrees, arcminutes, and arcseconds.

[b] Flux density at 4.85 GHz from GB6 (Gregory et al. 1996).

We observed using an on-off procedure with 5 minutes spent at both on and off positions, followed by 10 s integrations of the off position with and without noise-diode calibration signal. Throughout the run we also observed the continuum sources listed in Table 2 for gain calibration. Flux densities for the calibrator sources were from the GB6 catalog (Gregory et al. 1996).

For both polarizations, the system temperature during our observations was about 32 K. Based on the measurements of the calibrator sources, we obtained gain values for each polarization and for each observed sky position. The gains varied between 2–2.5 K Jy^{-1}. To convert our spectra to a Jy scale, we applied the measured telescope gains to the individual scans as a function of position on the sky and subsequently averaged the two polarizations and all scans on a particular source. Based on variations of the telescope gain we estimate our flux density calibration to be accurate to about 30%. For each source both on and off spectra were inspected individually, in order to check for absorption and/or emission in the off position and for presence of radio interference. The spectra are shown in Figure 1.

Line parameters were derived using the CLASS software package.[2] The H_2CO spectra were Hanning smoothed to a velocity resolution of 0.38 km s^{-1}. In most cases, line parameters were obtained using Gaussian fits. In cases where such fitting was not possible due to strong line asymmetries and complicated multipeaked structures, we list the velocity widths at zero power, and the LSR velocity and depth of the strongest absorption line in the complex. The H110α data were smoothed using box car averaging of width 10 channels, to a final velocity resolution of 1.88 km s^{-1}. H110α line parameters were obtained using a single Gaussian. Continuum emission was detected in most cases and its intensity was derived from the baseline in the H110α spectra. Continuum and H110α line parameters are given in Table 3, and H_2CO line parameters are given in Table 4.

3. RESULTS

3.1. *Kinematic Distances*

In all cases we find a H_2CO absorption line at an almost identical velocity to that of the H110α line, demonstrating that the H II regions are closely associated with molecular gas. We did not detect any systematic velocity trend between the associated molecular and ionized gas.

We derived kinematic distances for the H II regions from their RRL velocity and for the intervening molecular clouds from the H_2CO absorption lines. For this, we used the rotation curve of Brand & Blitz (1993), with $R_0 = 8.5$ kpc and $\Theta_0 = 220$ km s^{-1}. To determine kinematic distances from our data, we assume that all H_2CO absorption lines are produced by absorption of radio continuum from a single background H II region.

Based on these assumptions, if the H_2CO absorption occurs at higher velocities than the RRL, then the H II region has to be located at the far distance (e.g., Fig. 1*a*). This is the case for four sources in our sample. If no molecular gas was detected at velocities higher than the RRL, then the near kinematic distance is implied for the H II region (e.g., Fig. 1*e*). This is the case for seven sources in our sample.

A caveat is needed for the seven sources at the near kinematic distance. Implicit in their assignment to the near dis-

[2] CLASS is part of the GILDAS software developed by IRAM.

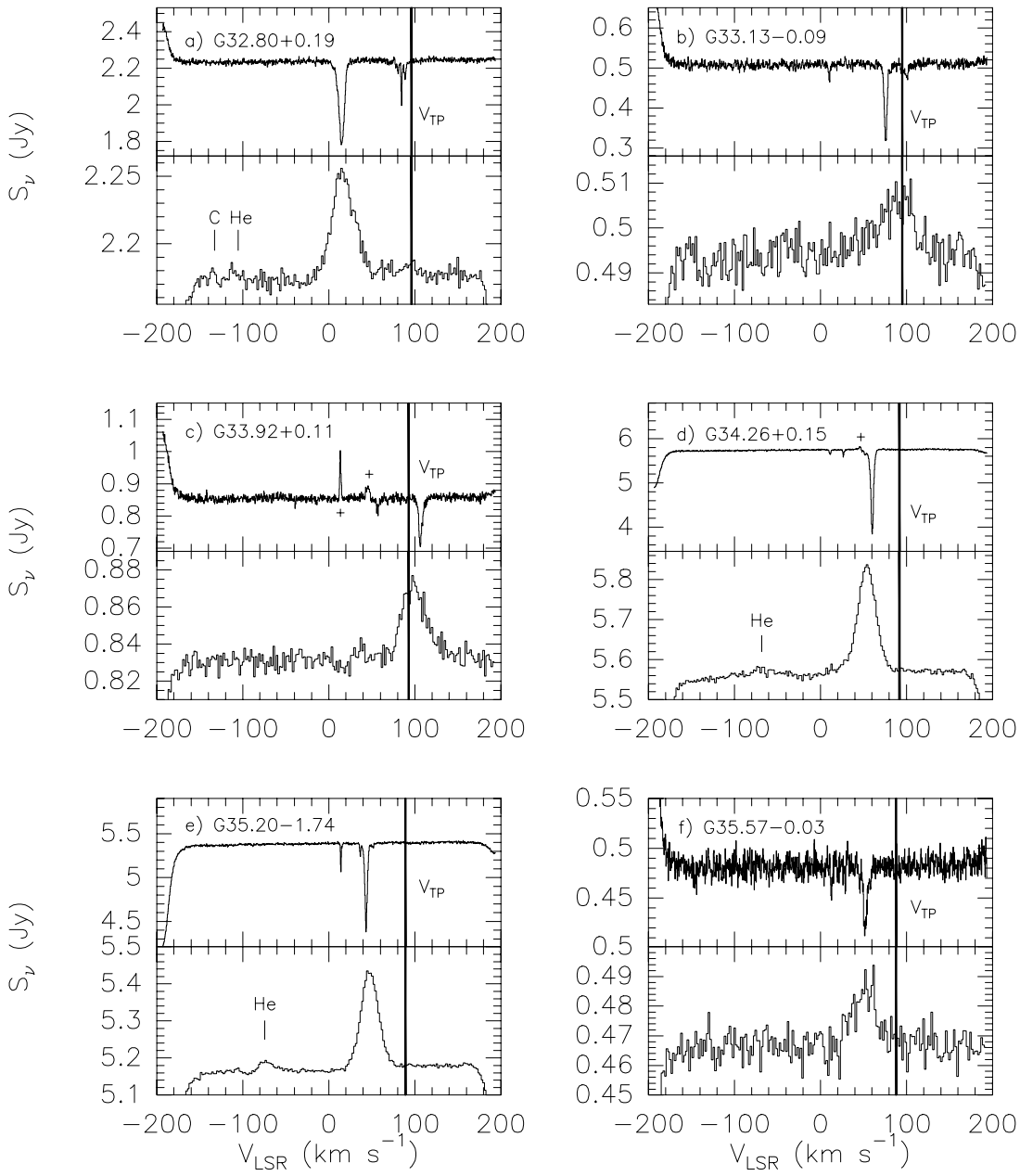

FIG. 1.—(*a–u*) Calibrated spectra obtained for 21 lines of sight in the Galactic plane. The H_2CO spectra are shown in the upper panels and the H110α spectra in the lower panels. A thick vertical line marks the tangent velocity. The positions of He110α and C110α are shown whenever detected. Artifacts in the spectra caused by H_2CO absorption in the reference position are marked with a cross (+).

tance is the assumption that the line of sight between the near and far kinematic positions does contain molecular gas. For widely separated near and far kinematic distances this is usually a good assumption, but as the two distances approach one another (and finally are equal at the tangent point) the assumption becomes less reliable. Kuchar & Bania (1990) observed H I toward G43.89−0.78 and found absorption at velocities higher than the RRL. Taking this into account, we report the far kinematic distance for this source in Table 5, thus, changing the number of "far" and "near" sources to five and six, respectively. The presence of this intervening atomic gas, where we found no molecular gas, serves to illustrate that the assumption of line-of-sight molecular gas may not always be valid.

We assigned 8 H II regions to the tangent point position, allowing deviations from the tangent velocity of up to ± 7 km s^{-1} due to noncircular motions (e.g., Fig. 1*n*). We found two sources with Galactocentric distance larger than 8.5 kpc, therefore these sources do not present distance ambiguity (e.g., Fig. 1*u*).

Kinematic distances to the intervening molecular clouds can also be determined. All molecular clouds with velocities less than that of the RRL are at the near kinematic distance (e.g., Fig. 1*l*). This is the case for 14 molecular clouds. When the formaldehyde absorption is at higher velocities than the RRL emission, the distance ambiguity for the molecular cloud cannot be resolved because the molecular gas could be on either side of the tangent point, at either the near or

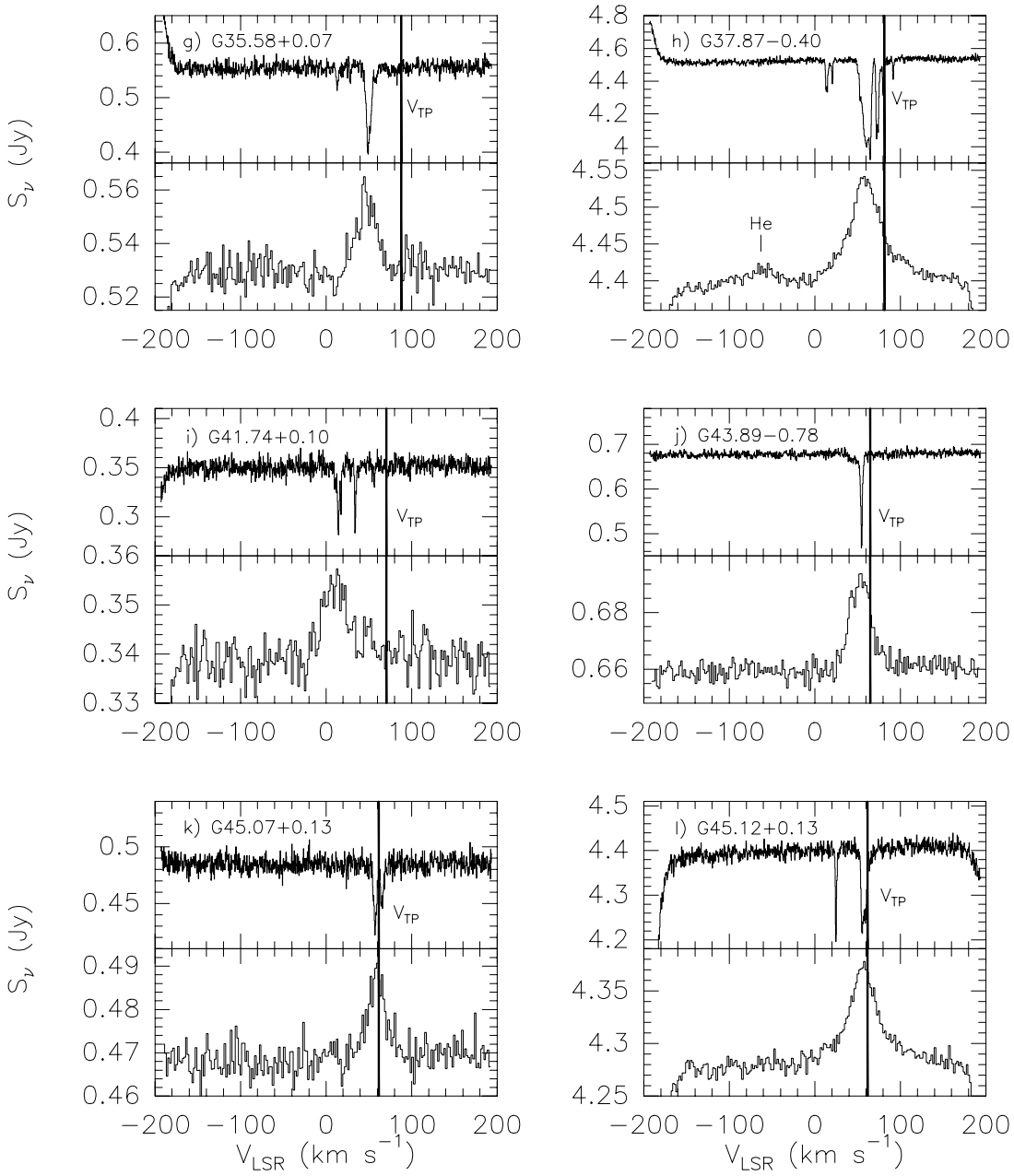

FIG. 1.—*Continued*

the far kinematic distance corresponding to its velocity. The kinematic distance to the absorbing molecular gas with velocity larger than that of the RRL is uniquely determined only if it is located at the tangent point. This is the case for five molecular clouds.

Applying these criteria with the assumptions outlined above, we resolve the distance ambiguity for all H II region in our sample, with the exception of G69.54+0.98, for which no H110α was detected. For this H II region we assigned a distance based on its H_2CO line. We also determined the Galactic location of 19 intervening molecular clouds. The results are presented in Table 5. Columns (1) and (2) list source name and measured LSR velocity, columns (3)–(6) list the near and far kinematic distances, the tangent point velocity, and distance to the tangent point based on the Brand & Blitz (1993) rotation curve, and columns (7), (8), and (9) list our results for the Galactocentric distance and the indicated kinematic distance.

We plot the Galactic location of both UCH II regions and molecular clouds in Figure 2. We include in this plot the H II regions from Georgelin & Georgelin (1976, hereafter GG76), with excitation-parameter greater than 200 pc cm^{-2} ("bright sources"). We calculate the kinematic position of the bright sources in the first Galactic quadrant, based on the Galactic rotation curve used in this work. GG76 report photometric distance of two bright H II regions, located in the fourth quadrant. We plot these two sources at the reported LSR distance. We scale the remaining bright H II regions of GG76 to a Sun Galactocentric distance of 8.5 kpc.

Figure 2 shows that the region surveyed in this work can be smoothly connected to the spiral arm structure suggested by GG76. However, in contrast to the usual assignment of spiral arms in the first quadrant (e.g., Downes et al. 1980) our data allow a different speculation: If the conspicuous linear structure between $l = 35°$–$48°$ is part of the

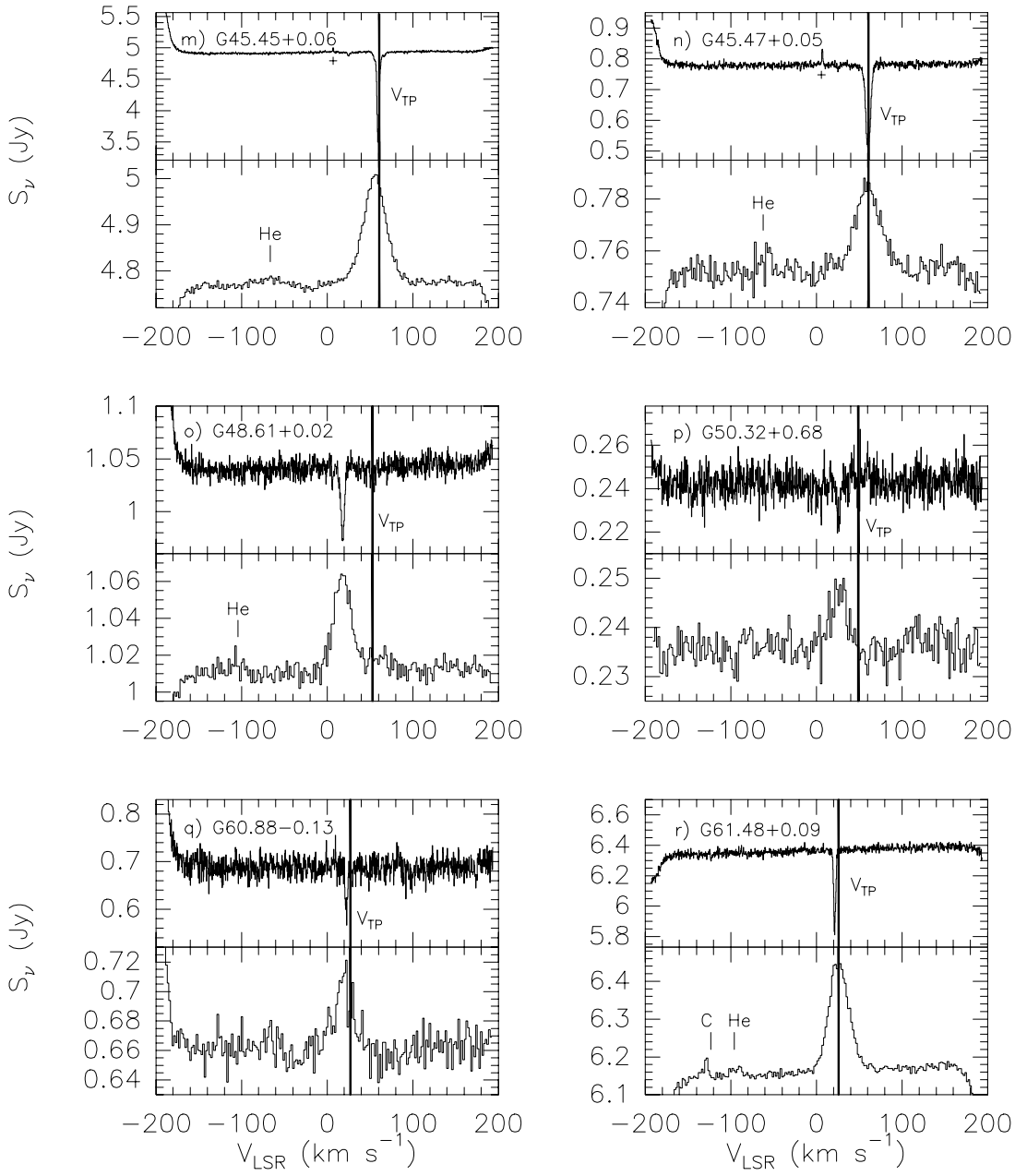

FIG. 1.—*Continued*

Sagittarius-Carina arm, then our data imply a strong change of pitch angle. This is what one might expect if the spiral arms originate at the end of a central bar, and in fact, this interpretation is consistent with the data of Weinberg (1992), who reports a stellar bar with semimajor axis of 5 kpc, semiminor axis of around 2.75 kpc and position angle of $-36° \pm 10°$ as seen from the Sun-Galactic center line. In Figure 2 we include an ellipse with the dimensions suggested in Weinberg (1992) but with a position angle of $-26°$.

3.2. *Extended Emission around* UCH II *Regions*

All of our target sources have previously been observed using radio interferometers with angular resolution between 0.″4 and 5″, giving flux densities for the ultracompact components. For 13 sources there are interferometric measurements at 6 cm wavelength, allowing direct comparison with the flux densities measured in the 1′ beam of the Arecibo telescope. For seven sources we have used existing interferometric measurements at 3.6 cm and 2 or 1.3 cm to estimate the flux density of the compact component at 6 cm by extrapolation using the measured spectral index. In cases where the spectral index was doubtful, we used a value of 0.6. Since UCH II regions are expected to become optically thick at wavelengths longward of 3.6 cm, the extrapolation should result in upper limits for the 6 cm flux density of the UCH II region.

We find that in general the flux densities measured with the Arecibo telescope are larger than those found with the VLA, the median value of $S_{\rm H\,II}/S_{\rm UCH\,II}$ being 3.0 (Fig. 3). Several sources have a single-dish to interferometer ratio exceeding 9. Thus, our data support the conclusion of Kurtz

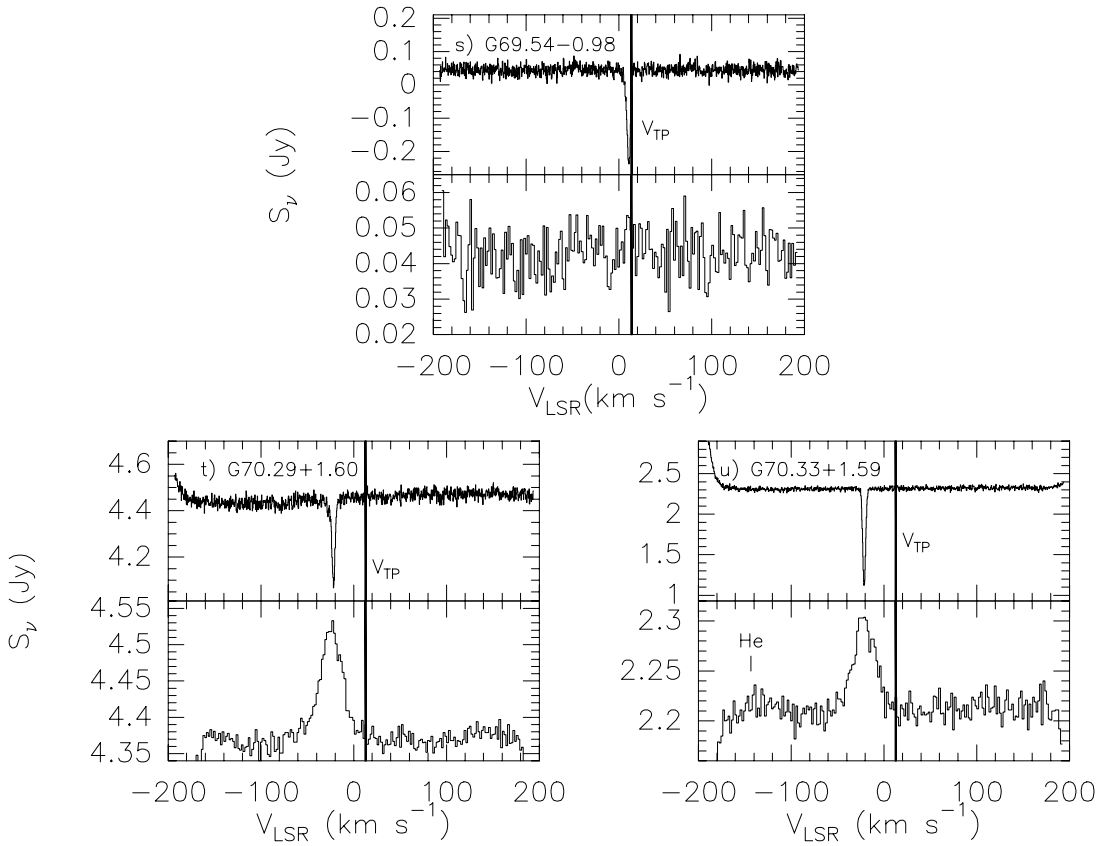

FIG. 1.—*Continued*

et al. (1999), and Kim & Koo (2001), that ultracompact H II regions are frequently associated with extended emission, which is missed by high resolution VLA observations.

The RRLs measured with the single-dish Arecibo beam of FWHM 1′ are likely dominated by the extended component of ionized gas largely because of beam dilution. Furthermore, the continuum optical depth of the ultracompact component may become appreciable at 6 cm which will

TABLE 3

H110α LINE AND CONTINUUM PARAMETERS

Source	S_c (Jy)	$S_{H110\alpha}$ (Jy)	V_{LSR} (km s^{-1})	FWHM (km s^{-1})	$\int S_v dv$ (Jy km s^{-1})	$S_{H\,II}/S_{UCH\,II}$
G32.80+0.19.....	2.176 (0.005)	0.075 (0.005)	16.9 (3.4)	30.1 (8.0)	2.4 (0.6)	1.47
G33.13−0.09.....	0.495 (0.003)	0.011 (0.003)	87.4 (2.0)	45.5 (4.7)	0.54(0.05)	2.06
G33.92+0.11.....	0.832 (0.004)	0.039 (0.004)	99.0 (0.6)	33.0 (1.5)	1.36 (0.05)	2.33
G34.26+0.15.....	5.565 (0.005)	0.263 (0.005)	54.0 (0.1)	25.5 (0.3)	7.14 (0.07)	3.52
G35.20−1.74.....	5.173 (0.004)	0.259 (0.004)	47.7 (0.1)	23.8 (0.3)	6.6 (0.1)	2.68
G35.57−0.03.....	0.467 (0.004)	0.019 (0.004)	51.8 (1.2)	31.9 (2.8)	0.65 (0.05)	1.37
G35.58+0.07.....	0.530 (0.005)	0.027 (0.005)	47.6 (0.8)	26.1 (1.9)	0.74 (0.05)	21.2
G37.87−0.40.....	4.401 (0.005)	0.127 (0.005)	59.2 (0.3)	47.3 (0.9)	6.37 (0.09)	2.37
G41.74+0.10.....	0.339 (0.003)	0.015 (0.003)	11.1 (1.2)	35.1 (3.3)	0.57 (0.04)	3.39
G43.89−0.78.....	0.660 (0.003)	0.032 (0.003)	53.4 (0.4)	28.4 (1.0)	0.96 (0.03)	1.80
G45.07+0.13.....	0.469 (0.003)	0.018 (0.003)	59.2 (0.8)	24.8 (2.1)	0.48 (0.03)	3.30
G45.12+0.13.....	4.282 (0.006)	0.083 (0.006)	56.7 (0.5)	44.5 (1.6)	3.9 (0.1)	3.67
G45.45+0.06.....	4.771 (0.006)	0.229 (0.006)	55.6 (0.2)	31.7 (0.5)	7.7 (0.1)	11.41
G45.47+0.05.....	0.752 (0.004)	0.032 (0.004)	60.1 (0.7)	34.5 (1.7)	1.2 (0.1)	9.52
G48.61+0.02.....	1.012 (0.004)	0.051 (0.004)	18.1 (0.4)	23.7 (1.0)	1.29(0.05)	9.46
G50.32+0.68.....	0.236 (0.003)	0.012 (0.003)	26.4 (1.1)	21.1 (2.5)	0.26 (0.03)	2.71
G60.88−0.13.....	0.662 (0.009)	0.043 (0.009)	19.0 (1.1)	24.3 (2.8)	1.1 (0.1)	28.8
G61.48+0.09.....	6.163 (0.007)	0.286 (0.007)	26.3 (0.1)	27.3 (0.3)	8.3 (0.1)	24.4
G69.54−0.98.....	...[a]	...[b]	...[b]	...[b]	...[b]	...[a]
G70.29+1.60.....	4.368 (0.130)	0.15 (0.01)	−24.2 (0.4)	29.1 (1.0)	4.7 (1.0)	1.28
G70.33+1.59.....	2.209 (0.010)	0.091 (0.010)	−21.1 (0.5)	28.0 (1.2)	2.7 (0.1)	0.69

NOTES.—1 σ statistical errors from the fit are presented in parentheses. Calibration errors are approximately 30%.

[a] Continuum emission in off position.

[b] No detection.

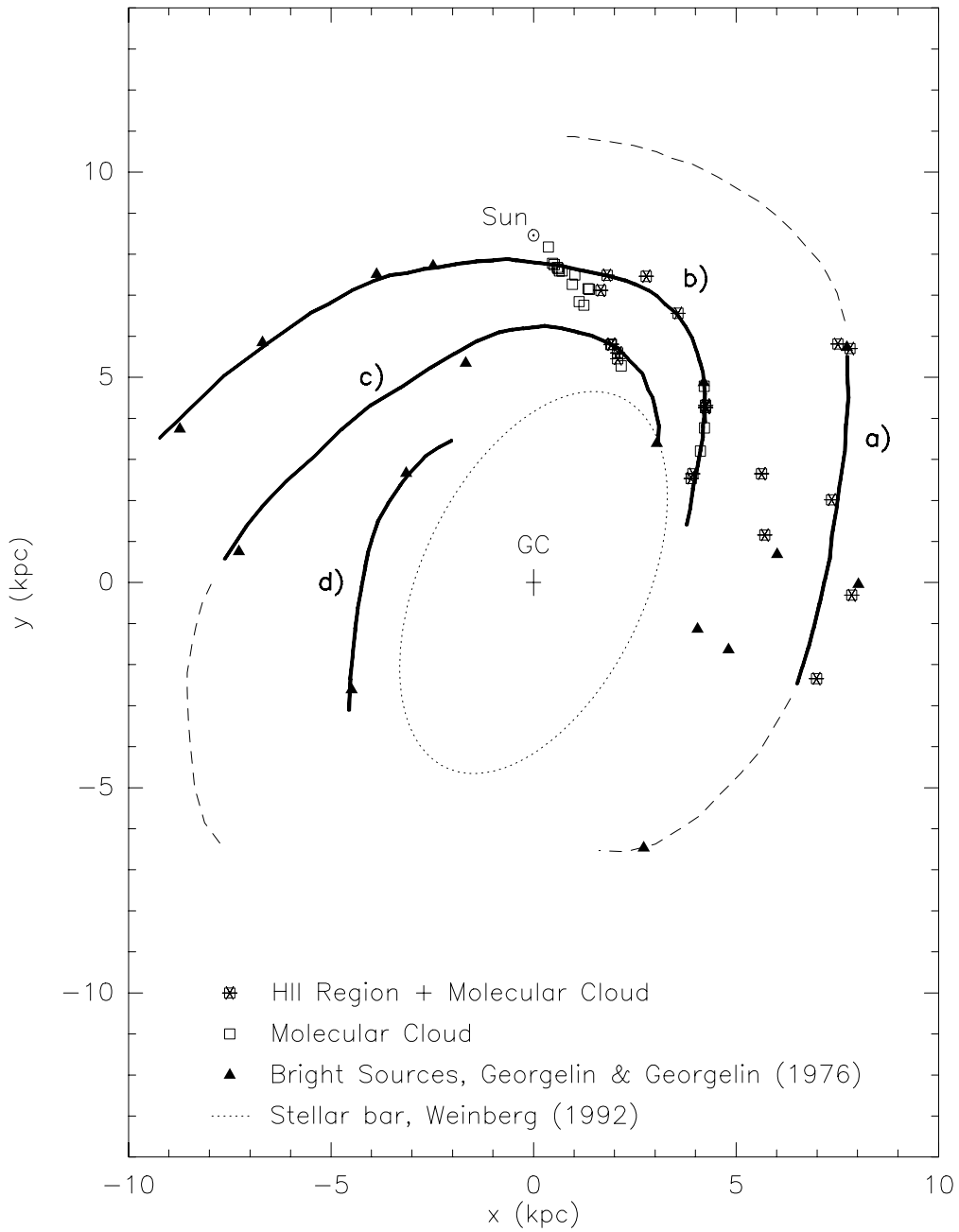

FIG. 2.—Spiral structure of the Galaxy derived from (1) H II regions presented by GG76 with excitation-parameter greater than 200 pc cm^{-2} ("bright" sources) and (2) the sources studied in this work. Note that every H II region in our sample has an associated molecular cloud. The kinematic distances to the GG76 H II regions were rescaled to a Sun Galactrocentric distance 8.5 kpc and the ones belonging to the first Galactic quadrant were calculated using the rotation curve used in this work. The central ellipse represents the stellar bar structure reported by Weinberg (1992). (*a*) Perseus arm, (*b*) Sagittarius-Carina arm, (*c*) Scutum-Crux arm, (*d*) Norma arm. The thick lines emphasize the suggested spiral pattern. Dashed lines represent a possible arm extrapolation.

reduce its contribution to the RRL measured with the Arecibo telescope. Thus, we are able to compare the velocity of the ionized gas in both, the extended and the ultracompact regions, providing an additional test of whether both components arise from the same physical region. For 10 sources of our sample, interferometric measurements of hydrogen RRLs (tracing the ultracompact component) are available from the literature. A comparison of the single-dish and interferometric observations shows that the velocity difference between extended and ultracompact ionized gas is smaller than about 4 km s^{-1} in 80% of the sources studied here. This supports the hypothesis that the extended emission does originate from the same star-forming region as the ultracompact component. However, we note that membership in the same-star forming region cannot determine if the regions are ionized by the same star, because distinct H II regions may have RRL velocities that differ by less than a few km s^{-1} (e.g., DePree et al. 1995). It appears that finding the stars responsible for the ionization of the region is necessary to determine whether the extended gas is physically related to the UCH II region or is caused by a different star.

TABLE 4

RESULTS H_2CO

Source	S_{H_2CO} (Jy)	V_{LSR} (km s^{-1})	Width (km s^{-1})	$\int S_v\,dv$ (Jy km s^{-1})	Notes
G32.80+0.19	−0.446(0.008)	14.878(0.026)	7.648(0.063)	−3.629(0.025)	G A
MC1a	−0.254(0.008)	84.613(0.023)	1.366(0.060)	−0.369(0.014)	4GMP E
MC1b	−0.090(0.008)	88.664(0.088)	3.213(0.312)	−0.308(0.021)	O
MC1c	−0.063(0.008)	80.626(0.129)	2.494(0.365)	−0.164(0.019)	O
MC1d	−0.045(0.008)	77.945(0.127)	1.079(0.226)	−0.051(0.012)	O
G33.13−0.09a	−0.192(0.007)	75.92(0.05)	3.80(0.12)	−0.77(0.02)	2GMP
G33.13−0.09b	−0.023(0.007)	81.62(0.35)	2.49(0.88)	−0.06(0.02)	O
MC1	−0.040(0.007)	101.5(0.4)[b]	11.3(0.8)	−0.25(0.05)	A V
MC2	−0.039(0.007)	10.39(0.08)	2.04(0.24)	−0.085(0.009)	G A
G33.92+0.11	−0.153(0.008)	106.4(0.4)	14.0(0.8)	−0.77(0.07)	MP V[a]
MC1	−0.055(0.008)	57.3(0.4)[b]	10.6(0.8)	−0.16(0.03)	MP V[a]
G34.26+0.15a	−1.828(0.015)	60.24(0.01)	3.80(0.03)	−7.39(0.06)	3GMP[a]
G34.26+0.15b	−0.126(0.015)	51.7			O
G34.26+0.15c	−0.047(0.015)	48.2			O
MC1	−0.160(0.015)	26.69(0.08)	1.04(0.22)	−0.176(0.031)	G A
MC2	−0.099(0.015)	11.25(0.19)	2.01(0.40)	−0.213(0.037)	G A
G35.20−1.74a	−1.018(0.008)	43.37(0.01)	3.672(0.023)	−3.34(0.05)	3GMP
G35.20−1.74b	−0.147(0.008)	36.67(0.10)	1.485(0.269)	−0.23(0.03)	O
G35.20−1.74c	−0.039(0.008)	50.47(0.68)	4.89(1.79)	−0.20(0.06)	O
MC1a	−0.324(0.008)	14.08(0.01)	0.934(0.027)	−0.322(0.008)	2GMP
MC1b	−0.059(0.008)	15.44(0.04)	0.53(0.18)	−0.033(0.006)	O
G35.57−0.03a	−0.064(0.009)	52.1(0.1)	4.60(0.30)	−0.311(0.016)	3GMP
G35.57−0.03b	−0.021(0.009)	45.6(0.3)	1.90(0.60)	−0.043(0.012)	O
G35.57−0.03c	−0.019(0.009)	57.6(0.5)	2.90(0.97)	−0.060(0.019)	O
MC1	−0.031(0.009)	12.8(0.2)	1.84(0.41)	−0.061(0.012)	G A
MC2	−0.031(0.009)	29.0(0.1)	0.81(0.20)	−0.027(0.007)	G A
G35.58+0.07a	−0.15(0.01)	49.3(0.4)[b]	18.5(0.8)	−1.09(0.07)	MP V
G35.58+0.07b	−0.12(0.01)	51.6(0.4)[b]			O
G35.58+0.07c	−0.03(0.01)	58.2(0.4)[b]			O
MC1	−0.03(0.01)	13.21(0.17)	2.80(0.40)	−0.102(0.013)	G A
G37.87−0.40a	−0.615(0.011)	64.9(0.4)[b]	21.3(0.8)	−6.4(0.2)	MP V
G37.87−0.40b	−0.536(0.011)	60.7(0.4)[b]			O
G37.87−0.40c	−0.253(0.011)	53.1(0.4)[b]			O
MC1a	−0.481(0.011)	72.4(0.4)[b]	13.9(0.8)	−2.2(0.1)	MP V
MC1b	−0.444(0.011)	74.3(0.4)[b]			O
MC1c	−0.223(0.011)	80.0(0.4)[b]			O
MC2a	−0.193(0.011)	14.9(0.4)[b]	11.4(0.8)	−0.86(0.11)	MP V
MC2b	−0.189(0.011)	13.5(0.4)[b]			O
MC2c	−0.143(0.011)	20.6(0.4)[b]			O
MC3	−0.123(0.011)	91.7(0.4)[b]	4.19(0.8)	0.16(0.06)	A V
G41.74+0.10a	−0.062(0.006)	14.57(0.14)	2.56(0.45)	−0.17(0.02)	3GMP
G41.74+0.10b	−0.043(0.006)	17.53(0.14)	1.13(0.39)	−0.05(0.01)	O
G41.74+0.10c	−0.020(0.006)	10.97(0.47)	2.51(0.88)	−0.05(0.02)	O
MC1	−0.066(0.006)	34.17(0.06)	1.63(0.14)	−0.12(0.01)	G A
MC2	−0.022(0.006)	56.47(0.13)	1.15(0.30)	−0.027(0.006)	G A
MC3	−0.019(0.006)	70.92(0.4)[b]	5.61(0.08)	−0.03(0.02)	MP V
G43.89−0.78a	−0.211(0.005)	54.6(0.4)[b]	20.7(0.8)	−0.76(0.07)	MP V
G43.89−0.78b	−0.023(0.005)	44.8(0.4)[b]			O
G45.07+0.13	−0.056(0.006)	57.49(0.10)	4.24(0.23)	−0.25(0.01)	G A
MC1	−0.036(0.006)	65.44(0.15)	4.09(0.34)	−0.16(0.01)	G A
G45.12+0.13a	−0.19(0.01)	55.6(0.4)[b]	16.6(0.8)	−1.38(0.03)	MP V
G45.12+0.13b	−0.18(0.01)	59.2(0.4)[b]			O
G45.12+0.13c	−0.05(0.01)	63.9(0.4)[b]			O

TABLE 4—*Continued*

Source	S_{H_2CO} (Jy)	V_{LSR} (km s^{-1})	Width (km s^{-1})	$\int S_v dv$ (Jy km s^{-1})	Notes
MC1.....	−0.20(0.01)	24.86(0.03)	1.68(0.08)	−0.36(0.01)	G A
G45.45+0.06	−1.42(0.01)	59.4(0.4)[b]	18.8(0.8)	−5.23(0.13)	A V[a]
MC1.....	−0.06(0.01)	24.96(0.13)	2.81(0.35)	−0.168(0.016)	G A
G45.47+0.05	−0.274(0.007)	60.48(0.03)	6.58(0.07)	−1.92(0.02)	G A[a]
MC1.....	−0.023(0.007)	25.2(0.4)[b]	3.76(0.8)	−0.039(0.016)	A V
G48.61+0.02	−0.067(0.007)	18.04(0.12)	4.96(0.28)	−0.35(0.02)	G A
MC1.....	−0.028(0.007)	53.8(0.4)[b]	2.0(0.8)	−0.06(0.01)	A V
MC2.....	−0.023(0.007)	6.07(0.49)	1.20(0.93)	−0.03(0.02)	G A
G50.32+0.68a	−0.023(0.006)	24.7(0.4)[b]	8.04(0.8)	−0.072(0.018)	MP V
G50.32+0.68b.....	−0.023(0.006)	26.6(0.4)[b]			O
G60.88−0.13	−0.093(0.018)	22.55(0.16)	3.23(0.36)	−0.319(0.032)	G A
G61.48+0.09	−0.531(0.015)	21.41(0.02)	2.81(0.05)	−1.59(0.02)	G A
G69.54−0.98	−0.280(0.014)	10.63(0.04)	4.53(0.10)	−1.353(0.027)	G A[c]
G70.29+1.60a	−0.372(0.019)	−21.725(0.050)	4.014 (0.131)	−1.5876(0.044)	2GMP A
G70.29+1.60b.....	−0.049(0.019)	−27.695 (0.018)	4.389 (1.119)	−0.228(0.047)	O
G70.33+1.59	−1.201(0.018)	−21.20(0.01)	3.65(0.02)	−4.66(0.03)	G

NOTES.—(MC) Intervening molecular cloud, arranged by decreasing line strength. (A) Asymmetric peak, not well fitted by Gaussian. (MP) Multipeak profile. (G) One Gaussian was used to fit the peak. (GMP) Number of Gaussians used to fit the multipeak line structure. Gaussian line parameters for the strongest peak are presented here. The other peaks fitted by the Gaussians could represent different molecular clouds. Its line parameters are presented in the following lines marked O (overlapped). If the Gaussian fit gave bad results for weaker components, we only report the approximate flux density and velocity of the overlapped line. (O) Overlapped with the previous peak. (V) Zero power width of the MP or A line is presented. The reported flux density and V_{LSR} correspond to the channel with deepest absorption. If we observe more than one peak within the complex, we present the approximate flux density and position of the overlapped peak in the following lines. (E) Possible emission line in this complex.

[a] For this spectrum, absorption is present in the off position.

[b] The V_{LSR} error presented is the channel width. The reported line width error is twice the channel width.

[c] No recombination line detected.

4. SUMMARY

Using the Arecibo Telescope we have observed the H110α radio recombination line and the H_2CO (1_{10}–1_{11}) rotational transition toward 21 UCH II regions. We have detected the H110α line in 20 of the 21 sources, and H_2CO absorption lines toward all. In every one of the 20 cases where H110α was detected, we have found a H_2CO line with nearly the same velocity, demonstrating that the UCH II regions are closely associated with molecular clouds. Absorption features at different velocities were also detected toward 14 of the H II regions in our sample.

Using the absorption features and a kinematic model of Galactic rotation, we resolve the distance ambiguity for all observed H II regions and 19 independent molecular clouds. For one of the H II regions, the distance is new determination.

A plot of H II regions and molecular cloud positions in the Galactic plane shows part of the first quadrant spiral structure of the Milky Way. Our results can be smoothly extrapolated to the spiral arms reported by GG76. However, our data suggest a rapid change of pitch angle in the first quadrant, consistent with the existence of a central bar structure.

We determine the ratio of the 6 cm continuum flux density between single-dish and interferometric measurements and find that our sample has a median ratio of 3.0. We also compare the H110α line velocity presented here with the UC H II region velocity available from the literature and find that the velocity difference between extended and ultracompact ionized gas is smaller than 4 km s^{-1} in 80% of the observed sources. This supports the idea that UCH II regions are associated with a spatially extended component of ionized gas.

We thank C. Salter and K. O'Neil for help during the observations, C. Salter for a critical reading of the manuscript, and J. Brand for providing an updated version of a rotation curve. We also thank the anonymous referee for comments which improved the manuscript. P. H. and E. A. acknowledge partial support from a UPR-DEGI grant, as well as NSF grant EPS-9874782. S. K. acknowledges support from UNAM DGAPA grant 117799.

TABLE 5

KINEMATIC PARAMETERS

Source (1)	V_{LSR} (km s^{-1}) (2)	D_{near} (kpc) (3)	D_{far} (kpc) (4)	V_{TP} (km s^{-1}) (5)	D_{TP} (kpc) (6)	D_{LSR} (kpc) (7)	D_{GC} (kpc) (8)	Notes[a] (9)
G32.80+0.19	16.9	1.35	12.9	95.7	7.14	12.9	7.40	Far
G32.80 MC1a.....	84.6	5.57	8.72	95.7	7.14	?	4.87	
G33.13−0.09	87.4	5.85	8.39	94.7	7.12	7.12	4.65	Tangent
G33.13 MC1	101.5	-	-	94.7	7.12	7.12	4.65	Tangent
G33.13 MC2	10.39	0.86	13.38	94.7	7.12	0.86	7.80	Near
G33.92+0.11	99.0	-	-	92.4	7.05	7.05	4.74	Tangent
G33.92 MC1	57.3	3.88	10.23	92.4	7.05	3.88	5.71	Near
G34.26+0.15	54.0	3.69	10.36	91.4	7.03	3.69	5.83	Near
G34.26 MC1	26.69	2.00	12.05	91.4	7.03	2.00	6.94	Near
G34.26 MC2	11.25	0.91	13.14	91.4	7.03	0.91	7.76	Near
G35.20−1.74	47.7	3.31	10.58	88.6	6.95	3.31	6.10	Near
G35.20 MC1a.....	14.08	1.11	12.78	88.6	6.95	1.11	7.62	Near
G35.57−0.03	51.8	3.57	10.26	87.5	6.91	3.57	5.97	Near
G35.57 MC1	12.8	1.01	12.81	87.5	6.91	1.01	7.70	Near
G35.57 MC2	28.98	2.14	11.69	87.5	6.91	2.14	6.87	Near
G35.58+0.07	47.6	3.31	10.51	87.5	6.91	3.31	6.12	Near
G35.58 MC1	13.21	1.05	12.8	87.5	6.91	1.05	7.67	Near
G37.87−0.40	59.2	4.12	9.30	80.9	6.71	9.30	5.82	Far
G37.87 MC2a.....	14.9	1.15	12.3	80.9	6.71	1.15	7.62	Near
G37.87 MC2c.....	20.6	1.56	11.9	80.9	6.71	1.56	7.33	Near
G37.87 MC3	91.72	-	-	80.9	6.71	6.71	5.22	Tangent(?)[b]
G41.74+0.10	11.1	0.86	11.8	70.1	6.34	11.8	7.88	Far (New Det)
G41.74 MC1	34.09	2.50	10.2	70.1	6.34	?	6.84	
G41.74 MC2	56.47	4.19	8.50	70.1	6.34	?	6.06	
G41.74 MC3	70.9	-	-	70.1	6.34	6.34	5.66	Tangent
G43.89−0.78	53.4	4.13	8.12	64.4	6.13	8.12	6.22	Far(?)[c]
G45.07+0.13	59.2	5.13	6.87	61.3	6.00	6.00	6.02	Tangent[d]
G45.07 MC1	65.44	-	-	61.3	6.00	6.00	6.02	Tangent
G45.12+0.13	56.7	4.72	7.27	61.2	6.00	6.00	6.02	Tangent[e]
G45.12 MC1	24.86	1.90	10.1	61.2	6.00	1.90	7.29	Near
G45.45+0.06	55.6	4.65	7.28	60.4	5.96	5.96	6.06	Tangent[e]
G45.45 MC1	24.96	1.43	9.80	60.4	5.96	1.43	7.07	Near
G45.47+0.05	60.1	5.68	6.24	60.3	5.96	5.96	6.06	Tangent[e]
G45.47 MC1	25.2	1.93	9.99	60.3	5.96	1.93	7.28	Near
G48.61+0.02	18.1	1.43	9.81	52.5	5.62	9.81	7.63	Far[f]
G48.61 MC1	53.8	-	-	52.5	5.62	5.62	6.38	Tangent
G48.61 MC2	6.07	0.49	10.6	52.5	5.62	0.49	8.19	Near
G50.32+0.68	26.4	2.16	8.69	48.5	5.43	2.16	7.31	Near[g]
G60.88−0.13	19.0	2.08	6.19	26.7	4.14	2.08	7.48	Near
G61.48+0.09	26.3	-	-	25.6	4.06	4.06	7.47	Tangent[h]
G69.54−0.98	10.63[i]	1.69	4.25	13.3	2.97	2.97	7.96	Tangent[j]

TABLE 5—*Continued*

Source (1)	V_{LSR} (km s^{-1}) (2)	D_{near} (kpc) (3)	D_{far} (kpc) (4)	V_{TP} (km s^{-1}) (5)	D_{TP} (kpc) (6)	D_{LSR} (kpc) (7)	D_{GC} (kpc) (8)	Notes[a] (9)
G70.29+1.60a.....	−24.2	-	-	12.4	2.87	8.30	9.67	
G70.33+1.59	−21.1	-	-	12.3	2.86	7.98	9.50	

[a] Kinematic location.

[b] Velocities larger than the tangent point velocity imply strong noncircular motions and/or undervalued velocities from the rotation curve. We tentatively assign this molecular cloud to the tangent distance.

[c] Kuchar & Bania 1990 report H I absorption at a higher velocity than the recombination line which implies the far kinematic distance. We detect no corresponding H_2CO absorption. Higher resolution and sensitivity H I emission-absorption observations should be obtained for confirmation.

[d] Contradictory distances are reported in the literature. Our result agrees with that of Churchwell et al. 1990.

[e] Radhakrishnan et al. 1972 present a H I spectrum, which shows absorption in the H I line wing up to 70 km s^{-1}, which would argue for the far distance (Downes et al. 1980). We prefer to assign the tangent distance.

[f] Kurtz et al. 1994 summarize previous discrepant distance determinations for this source. Our result agrees with the far kinematic distance.

[g] Churchwell et al. 1990 prefer to assign the far kinematic distance to G50.32+0.68 based on the trend of NH_3 line width and UV Luminosity as function of FIR Luminosity. We prefer to assign the near kinematic distance.

[h] Crampton et al. 1978 estimated a distance of 2 kpc to the nearby S88A region, based on a possible optical detection. Our results suggest that the kinematic position of S88B is at the tangent point.

[i] No recombination line detected. We use the H_2CO absorption line velocity.

[j] MacLeod et al. 1998 performed formaldehyde absorption observations toward this source which agree with our spectrum. They report the kinematic distance of this source as near. However, allowing for the possibility of noncircular motion, we prefer to assign the distance of tangent point.

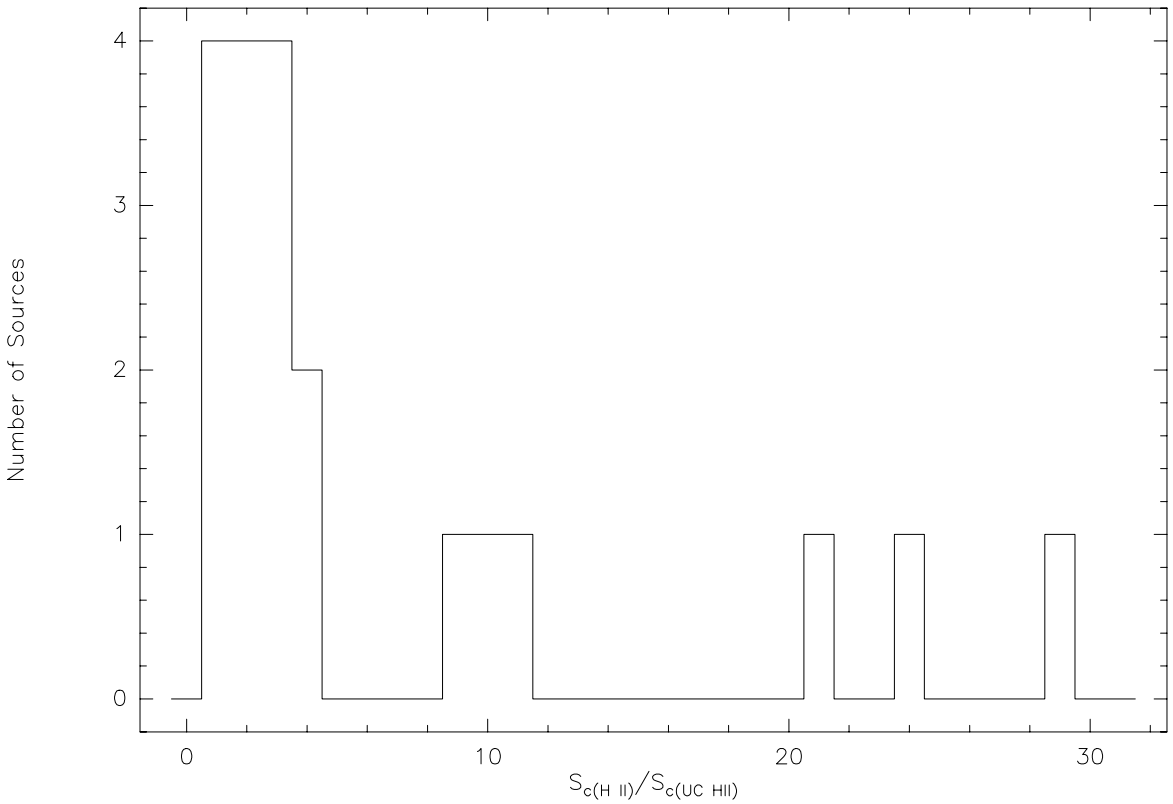

FIG. 3.—Histogram of the single-dish to interferometer 6 cm continuum flux density ratio S_{HII}/S_{UCHII}. The histogram bin width is equal to 1. The median is 3.0, suggesting that, in general, spatially extended radio continuum emission is present around UCH II regions and is missed by interferometric observations.

REFERENCES

Afflerbach, A., Churchwell, E., Acord, J. M., Hofner P., Kurtz, S., & DePree, C. G. 1996, ApJ, 106, 423
Brand, J.& Blitz, L. 1993, A&A, 275, 67
Churchwell, E. 1999, in The Origin of Stars and Planetary Systems, ed. C. J. Lada & N. D. Kylafis (Dordrecht: Kluwer), 515
Churchwell, E., Walmsley, C. M., & Cesaroni, R. 1990, A&A, 83, 119
Condon, J. J., Cotton, W. D., Greisen, E. W., Yin, Q. F., Perley, R. A., Taylor, G. B., & Broderick, J. J. 1998, AJ, 115, 1693
Crampton, D., Georgelin, Y. M., & Georgelin, Y. P. 1978, A&A, 66, 1
DePree, C. G., Rodríguez, L. F., Dickel, H. R., & Goss,W. M. 1995, ApJ, 447, 220
Downes, D., Wilson, T. L., Bieging, J., & Wink, J. 1980, A&A, 40, 379
Georgelin, Y. M., & Georgelin, Y. P. 1976, A&A, 49, 57 (GG76)
Gregory, P. C., Scott, W. K., Douglas, K., & Condon, J. J. 1996, ApJS, 103, 427
Kim, K. T., & Koo, B. C. 2001, ApJ, 549, 979
Kuchar, T. A., & Bania, T. M. 1990, ApJ, 352, 192
Kuchar, T. A., & Bania, T. M. 1994, ApJ, 436, 117
Kurtz, S., Cesaroni, R., Churchwell, E., Hofner, P., & Walmsley, C. M. 2000, Protostars and Planets IV, ed. V. Mannings, A. P. Boss, & S. S. Russell (Tucson: Univ. Arizona Press), 299
Kurtz, S. E., Churchwell, E., & Wood, D. O. S. 1994, ApJS, 91, 659
Kurtz, S. E., Watson, A. M., Hofner, P., & Otte, B. 1999, ApJ, 514, 232
Lim, J., & White, S. M. 1999, in Star Formation 1999, ed. T. Nakamoto (Nagano: Nobeyama Radio Obs.), 30
Lockman, F. J. 1989, ApJS, 71, 469
MacLeod, G. C., Scalise, E., Saedt, S., Galt, J. A., & Gaylard, M. J. 1998, AJ, 116, 1897
Radhakrishnan, V., Goss, W. M., Murray, J. D., & Brooks, J. W. 1972, ApJS, 24, 49
Roelfsema, P. R., Goss, W. M., & Geballe, T. R. 1988, A&A, 207, 132
Weinberg, M. D. 1992, ApJ, 384, 81
Wood, D. O. S., & Churchwell, E. 1989, ApJS, 69, 831